JJEE
Volume 1, Number 2, 2015
Pages 55-72
Jordan Journal of Electrical Engineering
ISSN (Print): 2409-9600, ISSN (Online): 2409-9619

A Novel Adaptive Hysteresis Current Controller for Active Power Filters

Eyad k. Almaita[1,a], Johnson A. Asumadu[2]

[1]Department of Electrical Power and Mechatronics Engineering, Tafila Technical University, Tafila, Jordan
[2]Department of Electrical and Computer Engineering, Western Michigan University, Michigan, USA
[a]e-mail: e.maita@ttu.edu.jo

Received: May 18, 2015 *Accepted: July 4, 2015*

Abstract— Hysteresis Current Control (HCC) is considered one of the most popular PWM techniques used in active power filters applications. The variable switching frequency is an associated problem with the conventional HCC. In this paper, a novel adaptive HCC algorithm is introduced. The proposed algorithm inherits the advantages of the conventional HCC algorithm and effectively mitigates the problem of the variable switching frequency, associated with the conventional HCC. The proposed algorithm uses a closed-loop control scheme to maintain a nearly constant switching frequency for a Hysteresis current controller. Although this algorithm was applied on shunt active power filters, it can be extended to other applications. The proposed algorithm is validated through simulation results using MATLAB/SIMULINK.

Keywords— Active power filter, adaptive, hysteresis current control, power quality, shunt.

I. INTRODUCTION

With the proliferation of nonlinear loads in the power system, harmonic pollution becomes a serious problem that affects the quality of power in both transmission and distribution systems. The problems caused by harmonics include malfunctioning of fuses or circuit breakers relays, heating of conductors and motors, insulation degradation, and communication interference [1]-[3].

Passive filters have been used to compensate for harmonic voltages and currents. Even though passive filters are cheap and easy to operate, they have low harmonic bandwidth, can be subjected to resonance, have large sizes, and are affected by source impedance [4]. However, active power filters (APFs), which are more dynamic, have been introduced as an effective means to overcome the problems associated with passive filters. An APF measures the distorted signal and, based on a harmonic detection algorithm, decomposes the distorted signal into its fundamental components and other harmonic components. The active filter then uses a power electronics based circuit to compensate for the harmonic components, the reactive power, and any other distortion (such as unbalanced waveforms) [5], [6].

One of the most crucial parts for the success of the compensating process by APFs is the PWM control technique used in APFs. The precise and fast control algorithms are required in order to achieve the sinusoidal current. Literature contains many algorithms used to drive the APF circuit [5]-[12]. The hysteresis current control (HCC) algorithm is considered one of the most suitable PWM algorithms because it is fast, easy to implement, accurate, and unconditionally stable [13]-[15]. The conventional HCC algorithm has a few drawbacks such as variable switching frequency and interference between phases in three phase case [16]-[20]. These drawbacks can drive the APF circuit to excessive switching, which can cause devices failure and increase switching losses. The literature introduces four main techniques used to tackle the problem of the variable switching frequency for the HCC algorithm: (i) space-vector based hysteresis current controllers [21], [22], (ii) adaptive hysteresis band

Corresponding author's e-mail: e.maita@ttu.edu.jo

current control technique [17], [23], (iii) fuzzy based hysteresis current controller [24], [25], and (iv) neural network based hysteresis current controller [26]-[29]. While many of the introduced algorithms reduce variation in the switching frequency, they add complexity to the basic HCC algorithm such as: the need to calculate the derivatives of load currents, overhead computations, or the use of the PLL. This complexity is not suitable for APFs applications.
This paper introduces a novel, effective, and easy-to-implement adaptive control algorithm for the HCC. The proposed algorithm uses a closed-loop control scheme that compares user-defined reference switching frequency with actual switching frequency, and then updates the hysteresis band to obtain nearly constant switching frequency.

II. SYSTEM ANALYSIS

Fig. 1 shows the system configuration of the Shunt Active Power Filter (SAPF). The main purpose of the SAPF is to compensate for current harmonics of the non-linear load; it cannot be used for compensating the harmonics of the voltage-source harmonics [28]. The SAPF is driven by a controller to draw a compensating current I_c from the source. This compensating current equals the sum of the harmonics and the reactive currents drawn by the non-linear load. Theoretically, the resultant source current (I_s) should be harmonic free and in-phase with the AC mains voltage [5], [6].

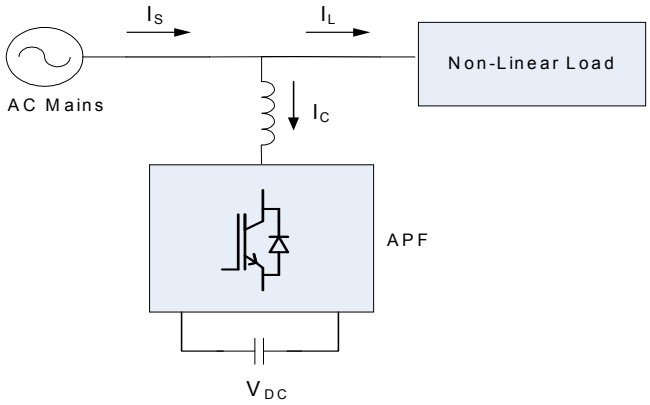

Fig. 1. SAPF block diagram

A. System Modeling

In order to derive the relation between the hysteresis band and switching frequency, the power circuit of the SAPF shown in Fig. 2 has been adopted. The SAPF is assumed to be connected to a balanced three-phase system as shown in Fig. 2. The switching transistors T_1 through T_6 are supposed to be driven by HCC unit.
By applying the Kirchhoff's voltage law, the following equations can be obtained:

$$V_{fa} = V_{f1} + V_{SN}$$
$$V_{fb} = V_{f2} + V_{SN} \quad (1)$$
$$V_{fc} = V_{f3} + V_{SN}$$

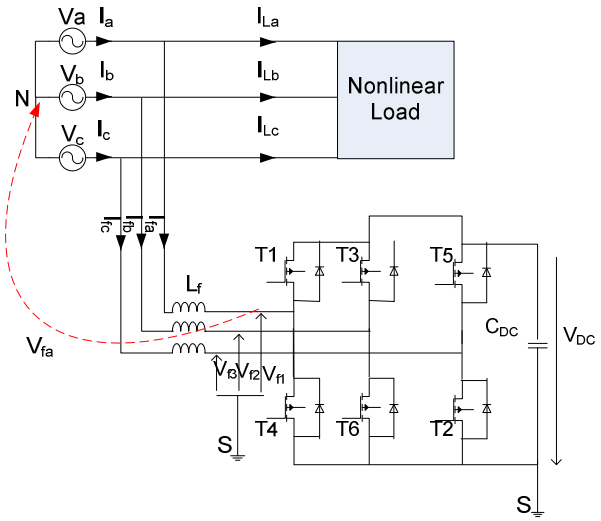

Fig. 2. VSI based three-phase shunt active power filter

Taking into account the balance three-phase system in (1), the S-point-to-neutral voltage is given by summing (1) as:

$$V_{SN} = -\frac{1}{3}\left(V_{f1} + V_{f2} + V_{f3}\right) \tag{2}$$

Substituting (2) into (1)

$$\begin{aligned} V_{fa} &= \frac{2}{3}V_{f1} - \frac{1}{3}V_{f2} - \frac{1}{3}V_{f3} \\ V_{fb} &= -\frac{1}{3}V_{f1} + \frac{2}{3}V_{f2} - \frac{1}{3}V_{f3} \\ V_{fc} &= -\frac{1}{3}V_{f1} - \frac{1}{3}V_{f2} + \frac{2}{3}V_{f3} \end{aligned} \tag{3}$$

Equation (3) can be rewritten in matrix form as:

$$\begin{vmatrix} V_{fa} \\ V_{fb} \\ V_{fc} \end{vmatrix} = \frac{1}{3}\begin{vmatrix} 2 & -1 & -1 \\ -1 & 2 & -1 \\ -1 & -1 & 2 \end{vmatrix}\begin{vmatrix} V_{f1} \\ V_{f2} \\ V_{f3} \end{vmatrix} \tag{4}$$

Based on a switching function (S_k), the voltages V_{f1}, V_{f2}, and V_{f3} can be switched between three values: 0, $+V_{DC}$, or $-V_{DC}$. The switching function (S_k) of the k^{th} inverter leg (k=1, 2, 3) can be defined as:

$$S_k = \begin{cases} 1, \text{if } \mathrm{T_j} \text{ is ON and } \mathrm{T_{j+3}} \text{ is OFF} \\ 0, \text{if } \mathrm{T_j} \text{ is OFF and } \mathrm{T_{j+3}} \text{ is ON} \end{cases} \quad \mathrm{j}=1,3,5 \tag{5}$$

The voltages V_{f1}, V_{f2}, and V_{f3} can be written as:

$$\begin{vmatrix} V_{f1} \\ V_{f2} \\ V_{f3} \end{vmatrix} = \begin{vmatrix} S_1 \\ S_2 \\ S_3 \end{vmatrix} V_{DC} \tag{6}$$

Substituting (6) into (4), the SAPF phase-to-neutral voltages can be expressed as:

$$\begin{vmatrix} V_{fa} \\ V_{fb} \\ V_{fc} \end{vmatrix} = \frac{1}{3} \begin{vmatrix} 2 & -1 & -1 \\ -1 & 2 & -1 \\ -1 & -1 & 2 \end{vmatrix} \begin{vmatrix} S_1 \\ S_2 \\ S_3 \end{vmatrix} V_{DC} \tag{7}$$

The switching vector [S_1 S_2 S_3] can have eight possible switching states and, based on these switching states, the voltages V_{fa}, V_{fb}, and V_{fc} can be switched between five values as shown in Table 1.

TABLE 1
POSSIBLE SWITCHING STATES AND THE CORRESPONDING VALUES OF THE VOLTAGES

State #	S_3	S_2	S_1	V_{fa}	V_{fb}	V_{fc}
1	0	0	0	0	0	0
2	0	0	1	2/3 V_{DC}	-1/3 V_{DC}	-1/3 V_{DC}
3	0	1	0	-1/3 V_{DC}	2/3 V_{DC}	-1/3 V_{DC}
4	0	1	1	1/3 V_{DC}	1/3 V_{DC}	-2/3 V_{DC}
5	1	0	0	-1/3 V_{DC}	-1/3 V_{DC}	2/3 V_{DC}
6	1	0	1	1/3 V_{DC}	-2/3 V_{DC}	1/3 V_{DC}
7	1	1	0	-2/3 V_{DC}	1/3 V_{DC}	1/3 V_{DC}
8	1	1	1	0	0	0

The variation in the voltages V_{fa}, V_{fb}, and V_{fc} during the switching period makes the derivation of the relation between the hysteresis band and the switching frequency difficult. For simplicity the average values of the voltages V_{fa}, V_{fb}, and V_f during one switching interval (TR or TF) are adopted as in [17]. Fig. 3 shows the average rising and falling current inside the hysteresis band in a conventional HCC, which is used to control the SAPF in Fig. 2. The differential equations of the phase a current I_a for the intervals TR and TF can be expressed as:

$$L_f \frac{dI_{fa}^R}{dt} = Q_{fa} V_{DC} - V_a \tag{8}$$

$$L_f \frac{dI_{fa}^F}{dt} = -Q_{fa} V_{DC} - V_a \tag{9}$$

$$\frac{dI_{fa}^R}{dt} + \frac{dI_{fa}^F}{dt} = 0 \tag{10}$$

where L_f is the coupling inductor of the SAPF, $I_{fa}{}^R$ and $I_{fa}{}^F$ are the respective average rising and falling current segments, $Q_{fa}V_{DC}$ is the average applied voltage during either the rising or falling segment (assumed to be the same), and V_a is the source voltage of the phase a measured at the connection point.

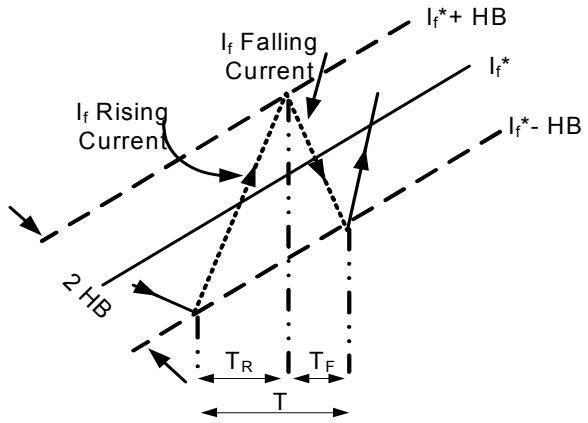

Fig. 3. Average rising and falling current

From the geometry of Fig. 3, the following equations can be derived:

$$\frac{dI_{fa}^{R}}{dt}T_R - \frac{dI_{fa}^{*}}{dt}T_R = 2HB \tag{11}$$

$$\frac{dI_{fa}^{F}}{dt}T_F - \frac{dI_{fa}^{*}}{dt}T_F = -2HB \tag{12}$$

$$T_R + T_F = T = \frac{1}{F_S} \tag{13}$$

Adding (11) and (12) and using (13) would result in the following equation:

$$\frac{dI_{fa}^{R}}{dt}T_R + \frac{dI_{fa}^{F}}{dt}T_F - \frac{1}{F_S}\frac{dI_{fa}^{*}}{dt} = 0 \tag{14}$$

Subtract (12) from (11):

$$\frac{dI_{fa}^{R}}{dt}T_R - \frac{dI_{fa}^{F}}{dt}T_F - (T_R - T_F)\frac{dI_{fa}^{*}}{dt} = 4HB \tag{15}$$

Substitute for $\frac{dI_{fa}^{F}}{dt}$ from (10) into (15):

$$4HB = (T_R + T_F)\frac{dI_{fa}^{R}}{dt} - (T_R - T_F)\frac{dI_{fa}^{*}}{dt} = \frac{1}{F_S}\frac{dI_{fa}^{R}}{dt} - (T_R - T_F)\frac{dI_{fa}^{*}}{dt} \tag{16}$$

Substitute for $\frac{dI_{fa}^{F}}{dt}$ from (10) into (14) and simplify:

$$(T_R - T_F) = \frac{\frac{dI_{fa}^{*}}{dt}}{F_S\frac{dI_{fa}^{R}}{dt}} \tag{17}$$

Substitute (17) into (16):

$$4HB = \frac{1}{F_S}\left[\frac{dI_{fa}^{R}}{dt} - \frac{\left(\frac{dI_{fa}^{*}}{dt}^{2}\right)}{\frac{dI_{fa}^{R}}{dt}}\right] \tag{18}$$

Substitute for $\frac{dI_{fa}^{R}}{dt}$ from (8) into (18) and simplify:

$$F_S = \frac{Q_{fa}V_{DC}-V_a}{4HBL_f}\left[1-\frac{m^2{L_f}^2}{\left(Q_{fa}V_{DC}-V_a\right)^2}\right] \quad (19)$$

where $m = \frac{dI_{fa}^{*}}{dt}$ is the slope of the reference current.
Equation (19) shows the viability of maintaining the switching frequency (F_s) constant if the hysteresis Band (HB) is modulated to minimize the effect of the variation in the slope of the reference current (m), the phase voltage (V_a), and the supply voltage ($Q_{fa}V_{DC}$).

B. Conventional HCC Algorithm

Fig. 4 shows how the conventional HCC algorithm works. It depends on the current error (ΔI) between the reference current (I_c^*) and the actual current (I_c); if this difference exceeds any boundary of the hysteresis band the switching state will be toggled as follows:

$\Delta I = I_c^* - I_c$

If $I_c < I_c^* - HB$ *or* $\Delta I > HB$ then Output=1(ON)

This means that if the actual current is below the permissible value, the upper side transistor of the APF (i.e. T_1, T_3, or/and T_5) will be turned ON and the lower side transistor of the APF (i.e. T_4, T_6, or/and T_2) will be turn OFF. This action will connect the load to the positive DC side and cause the actual current to rise and bring it back within the hysteresis band.

If $I_c > I_c^* + HB$ or $\Delta I < -HB$ then Output=0(OFF)

This means that if the actual current is above the permissible value, the upper side transistor of the APF (i.e. T_1, T_3, or/and T_5) will be turned OFF and the lower side transistor of the APF (i.e. T_4, T_6, or/and T_2) will be turned ON. This action will connect the load to the negative DC side and cause the actual current to fall and bring it back within the hysteresis band.
The switching period (T) is given by:

$$T = T_{ON} + T_{OFF}$$

where T_{ON} is the time while the switch is on and T_{OFF} is the time while the switch is off.
Also, the switching frequency (F_S) is given as:

$$F_S = \frac{1}{T}$$

In conventional HCC, two successive switching periods are not necessarily equal. This inequality in switching periods results from two reasons: (i) the rising and the falling slope of I_c are dependent on system parameters, (ii) it can be affected by the other phases' interference in the case of three-phase systems. Those reasons make the conventional HCC suffer from variable switching frequency.

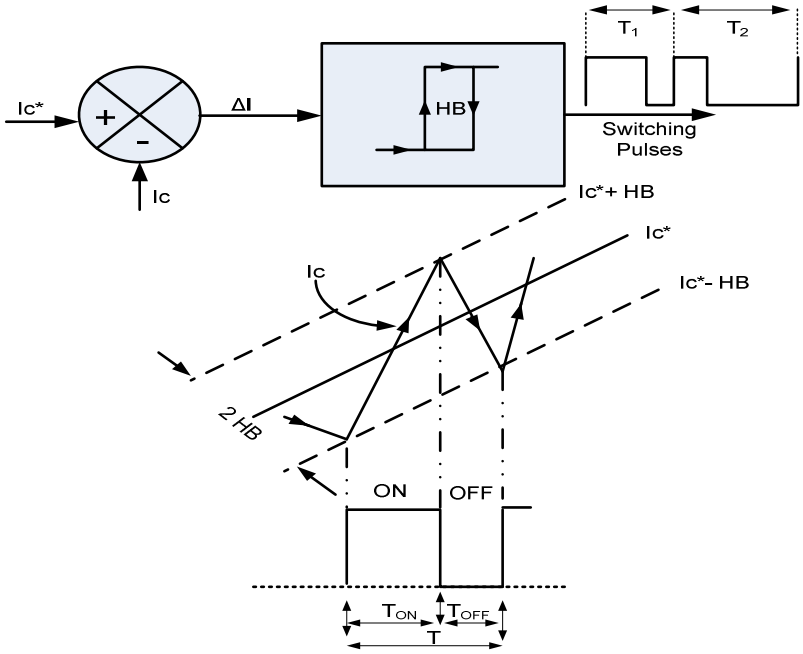

Fig. 4. Conventional hysteresis current control algorithm

III. PROPOSED ADAPTIVE HCC ALGORITHM

Fig. 5 shows the block diagram for the proposed algorithm. The proposed algorithm inherits all the good merits of the conventional HCC algorithm because this algorithm is built around a conventional HCC algorithm with the modulation capability for the hysteresis band. It does not need any information about system parameters. Unlike other algorithms used to tackle the variable switching frequency in conventional HCC, it preserves the simplicity of the conventional HCC algorithm which makes it easy to be implemented. Also, this algorithm provides a direct measurement for the actual switching frequency. This makes it possible to build closed-loop control systems where continuous assessments for the algorithm performance can be achieved.

Two counters are used to implement this algorithm: (i) asynchronous counter, the output of the counter depends on asynchronous clock, (ii) synchronous counter, the output of the counter depends on synchronous clock. The proposed closed-loop scheme uses the output pulses of hysteresis current unit as the input clock of an asynchronous counter as shown in Fig. 5. The output of the asynchronous counter, which is related to the actual switching frequency, is compared to the output of a synchronous counter, which is related to the reference switching frequency. The difference between the counters outputs is used to modulate the hysteresis band.

Fig 6 shows the flow diagram of the proposed adaptive HCC algorithm. A conventional HCC, with a variable hysteresis band, is used to drive a three-phase SAPF. The error (E) between the output of the reference synchronous counter and the output of asynchronous counter, driven by the pulses of the conventional HCC, is calculated as:

$$E = N_{ref} - N_{act} \tag{20}$$

where N_{ref} is the output of the reference synchronous counter and N_{act} is the output of the asynchronous counter.

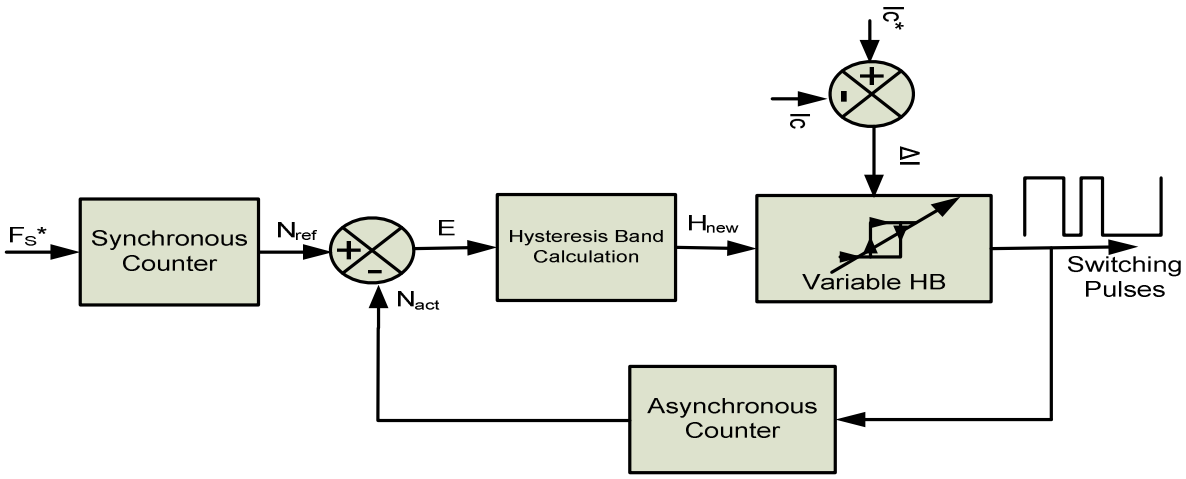

Fig. 5. Proposed adaptive HCC algorithm block diagram

While the error between these counters is zero, the controller will act as a conventional HCC. Once there is a mismatch between the two counters, the controller calculates a new value for the hysteresis band based on the sign. The value of that error is:

$$HB_{new} = HB_{old} - \eta * E \tag{21}$$

where HB_{new} is the new calculated hysteresis band, HB_{old} is the old hysteresis band, and η is a regulation factor obtained based on experience or by trial and error.

If the new calculated hysteresis band exceeds a preset values for the upper (*ULim*) and lower (*LLim*) limits of the hysteresis band, the controller takes the limit value as the new value for the hysteresis band. Otherwise, the controller will adopt this value as the new hysteresis band.

To illustrate the proposed HCC algorithm, the following numerical example shows how the proposed algorithm updates the hysteresis band for a given scenario. If the following scenario is assumed:

HB_{old}=14A, *ULim*=25A, *LLim*=0.1A, N_{ref}=3, N_{act}=5, I_{ref}=300A, I_{actual}=315A, η=0.75A, and the hysteresis band output will be 1 (ON).

According to the proposed algorithm, the error *E* can be calculated as:

$$E = N_{ref} - N_{act} = 3 - 5 = -2$$

This means the switching frequency is higher than the reference frequency and it needs to be adjusted. The new hysteresis band HB_{new} can be calculated as:

$$HB_{new} = HB_{old} - \eta * E = 14 - 0.75 * -2 = 15\text{A}$$

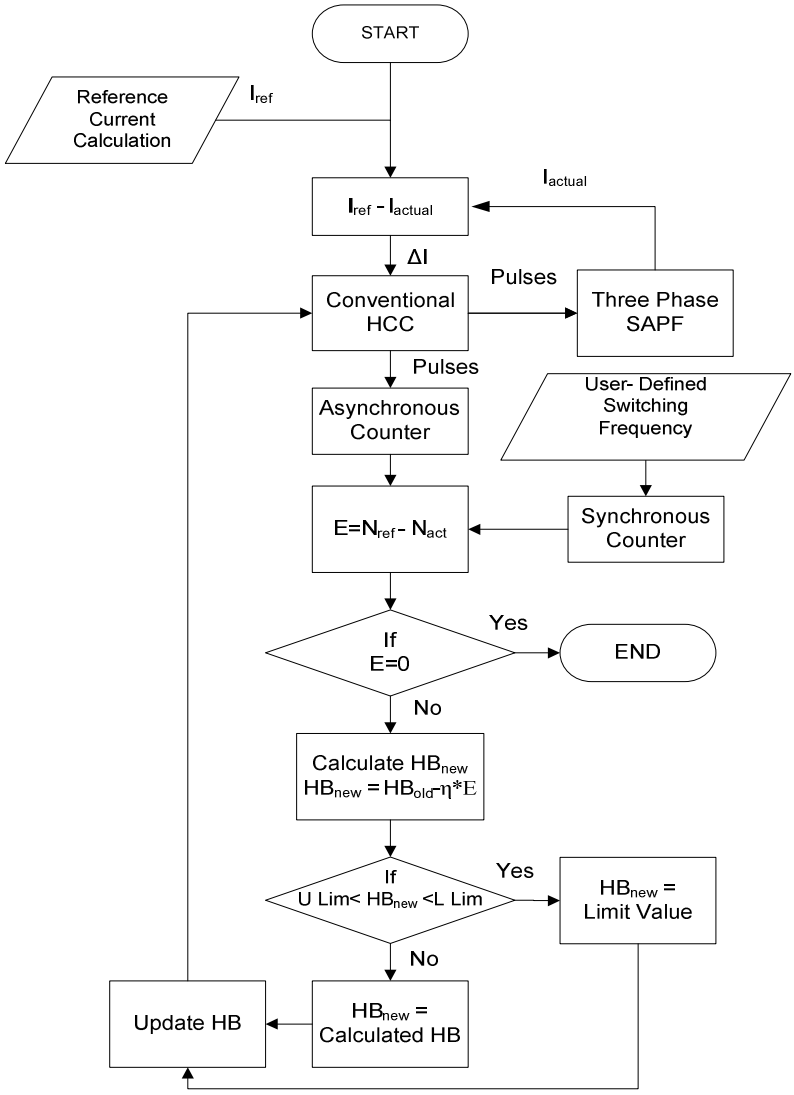

Fig. 6. Flow diagram of the adaptive RBFNN algorithm

The HB_{new} is within the upper (*ULim*) and lower (*LLim*) limits. The calculated HB_{new} will be adopted; and the hysteresis band will be updated to be 15A. The current error (ΔI) is calculated as:

$$\Delta I = I_{ref} - I_{actual} = 300 - 315 = -15\text{A}$$

To see the effect of the new algorithm, the following cases are considered:

- With conventional HCC algorithm:

The HB_{old} cannot be updated and will remain equal to 14A, so with ΔI<-*HB*=-15<-14 the Output=0 (OFF). The hysteresis current controller will toggle its state, the output will be 0 (OFF) and the switching frequency will remain the same.

- With proposed HCC algorithm:

The HB_{old} will be updated to the value 15A, so ΔI now is $-HB<\Delta I<HB$=-15<-15<15 the Output=remain the same 1 (ON). The hysteresis current controller will keep its current state and the output will be 1(ON). As a result, the switching duration T_{ON} and T will increase and the switching frequency will decrease because

$$F_S=1/T$$

IV. SIMULATION RESULTS

The proposed algorithm was used to control a SAPF system. The reference current was generated using the *p-q* theory as illustrated in the Appendix. For simplicity, the capacitor of the dc side of the SAPF is replaced by a constant voltage dc battery. The SAPF system has the following parameters:

Voltage Source:	400V L-L, 60Hz , source resistance 0.06mΩ, source inductance 2μH
Nonlinear Load:	Three-phase thyristor rectifier with *R-L* load (450kW active power, 200kVAR reactive power)
Sampling Rate:	5120 sample/cycle
Ref. cycles #:	3 cycles

Fig. 7(a) shows the actual current of the SAPF and Fig. 7(b) shows the reference current. The Fig. shows the ability of the proposed algorithm to track the reference current. Fig. 8 shows the source current. It can be seen that the source current becomes almost sinusoidal the moments the SAPF is ON. The noise in this current can be easily filtered out by an external passive filter.

The performance of the proposed algorithm can be measured by comparing it with a conventional HCC for the same system parameters. The band width for the conventional HCC was set to 0.1 and the proposed algorithm was to move between a value of 0.1 as a lower limit and a value of 30A as an upper limit.

Fig. 9 shows the performance of both the conventional HCC and the proposed algorithm to maintain a 7kHz reference switching frequency. The performance criterion was set based on measuring the error between the reference counter output, as shown in Fig. 5, and (i) the counter driven by the conventional HCC and (ii) the proposed algorithm. This error is calculated and plotted against a reference line. The Mean Square Error (MSE) for both algorithms was calculated. The proposed algorithm has a smaller (MSE= 9.93) compared to the conventional one (MSE= 303).

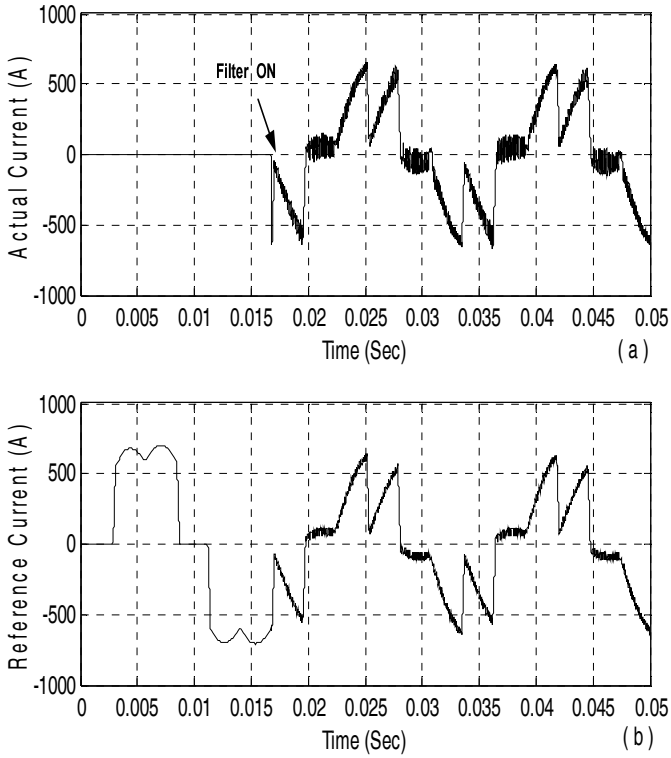

Fig. 7. SAPF output current: actual current (a) versus reference current (b)

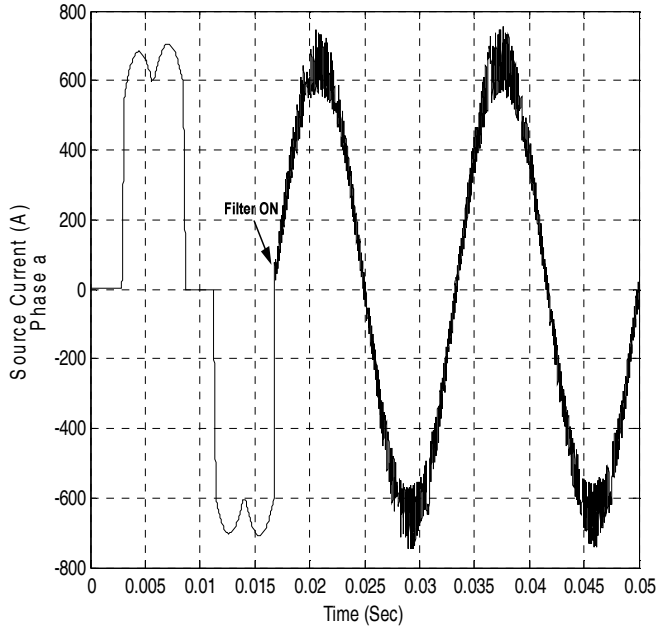

Fig. 8. Source current: phase a

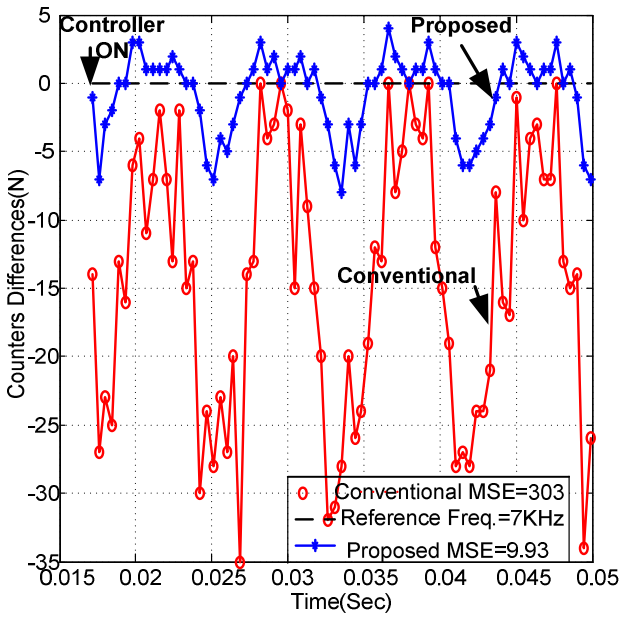

Fig. 9. Performance of both proposed algorithm (MSE=9.93) and the Conventional (MSE=303)

The consequence of the upper limit existence in the proposed algorithm is investigated in Fig. 12. It can be seen that for a 7-kHz reference switching frequency, the MSE for performance of the proposed algorithm with upper limit is greater than the one without upper limit. But the importance of this limit is the permissible current error in this algorithm as illustrated in Fig. 10.

Fig. 13 shows an example of the effect of the upper limit value on the performance of the proposed algorithm. It shows that for a 10-kHz reference switching frequency, as the upper limit value goes up, the MSE will be reduced.

Fig. 14 shows the effect of the regulation factor (LR) on the performance of the proposed algorithm. Even though the MSE's for the three tested values of the regulation factor (0.1, 0.5, and 1) were close, it can be seen that a reasonable higher regulation factor can help prevent an excessive switching frequency and enhance the fast response of the proposed algorithm.

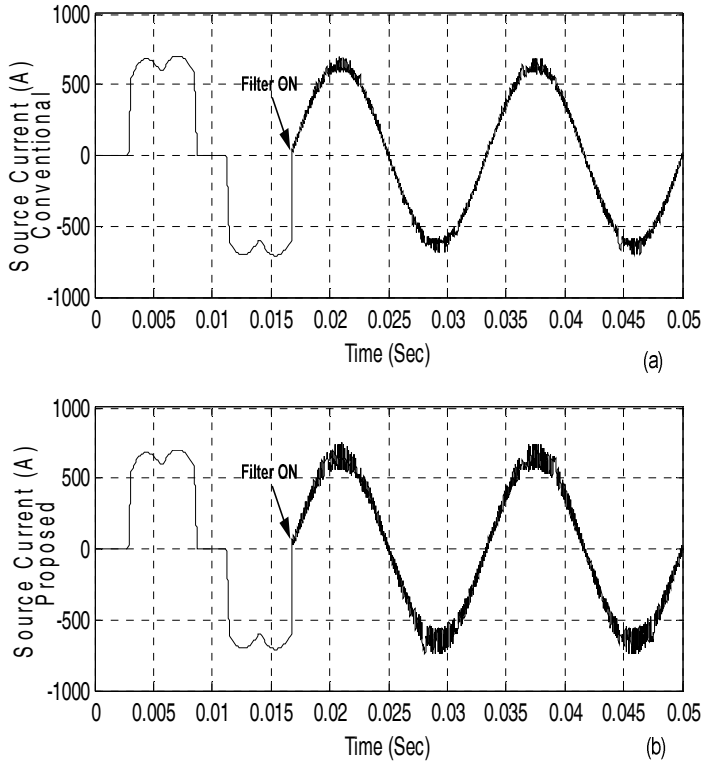

Fig. 10. Source current for the phase "a" conventional HCC (a) and adaptive HCC algorithm (b)

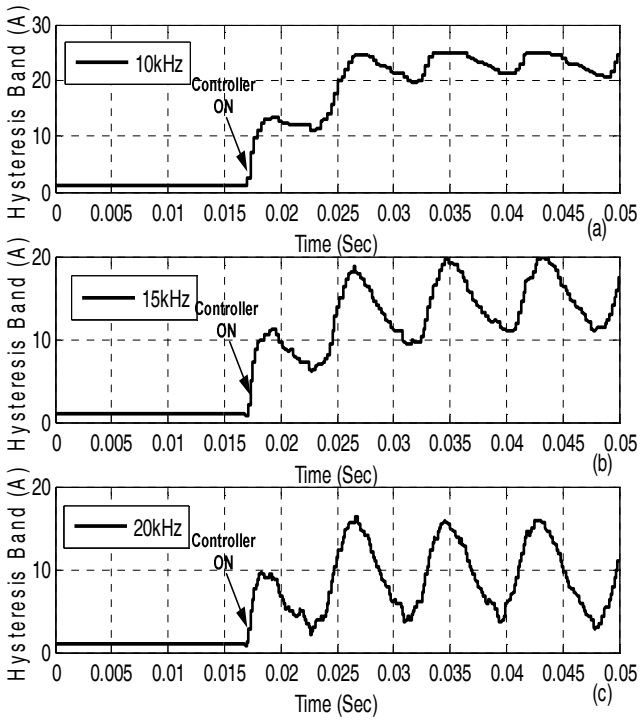

Fig. 11. Adaptive hysteresis band variation for different reference frequencies: (a) 10kHz (b) 15kHz (c) 20kHz

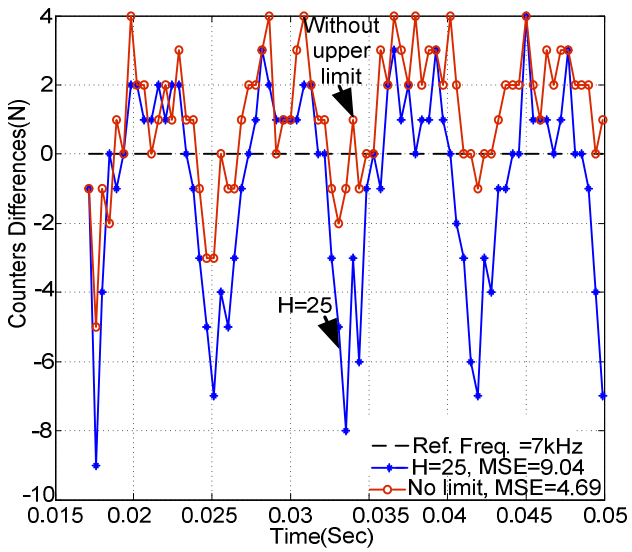

Fig. 12. Performance of the proposed algorithm with and without upper limit for the hysteresis band

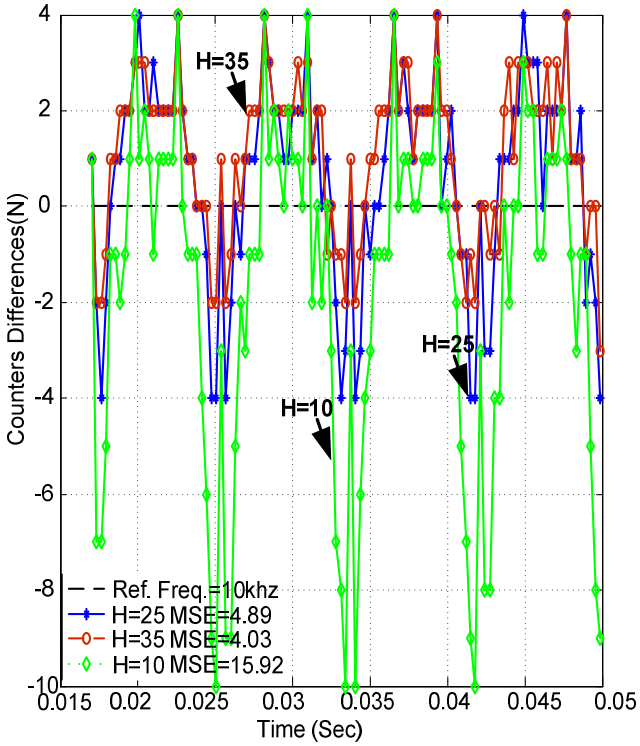

Fig. 13. Performance of the proposed algorithm for different values of the upper limits of the hysteresis band

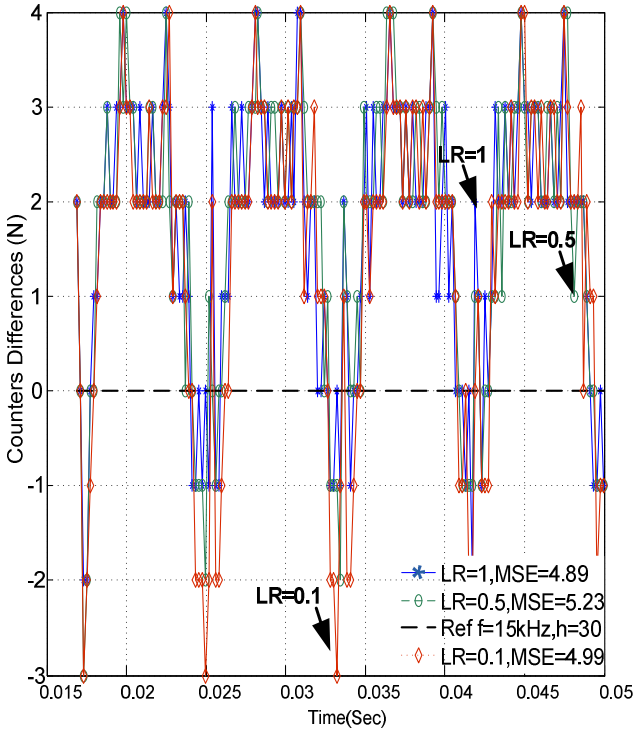

Fig. 14. Performance of the proposed algorithm for different regulation factor values: LR=0.1, MSE=4.99; LR=0.5, MSE=23; and LR=1, MSE= 4.89

V. CONCLUSIONS

A novel adaptive hysteresis band current controller is presented in this paper. The proposed algorithm nearly maintains a constant switching frequency for the HCC controller. The proposed algorithm uses simple and easy to implement closed-loop control schemes to build the controller. It uses the difference between the readings of two counters, which are related to the reference and actual switching frequencies, to modulate the hysteresis band. The sensitivity of the proposed algorithm for different parameters is investigated. The dynamic response of the proposed algorithm for different changes shows the effectiveness of the proposed algorithm. Also, the proposed algorithm can be extended to different application such as motors drive applications.

APPENDIX

p-q Theory: consider the three-phase controlled rectifier with R-L load as shown in Fig. A. A uniformly distributed random gating signal is applied to the three-phase rectifier. The voltages and currents of the rectifier are sampled and used to calculate the instantaneous active power *p* and imaginary power *q* based on *p-q* theory [30]. Clark transformation is used to transform the voltages and currents from *a-b-c* domain to *α-β* domain as shown in (22) and (23).

$$\begin{vmatrix} v_\alpha \\ v_\beta \end{vmatrix} = \sqrt{\frac{2}{3}} \begin{vmatrix} 1 & -\frac{1}{2} & -\frac{1}{2} \\ 0 & \frac{\sqrt{3}}{2} & -\frac{\sqrt{3}}{2} \end{vmatrix} \begin{vmatrix} v_a \\ v_b \\ v_c \end{vmatrix} \tag{22}$$

$$\begin{vmatrix} i_\alpha \\ i_\beta \end{vmatrix} = \sqrt{\frac{2}{3}} \begin{vmatrix} 1 & -\frac{1}{2} & -\frac{1}{2} \\ 0 & \frac{\sqrt{3}}{2} & -\frac{\sqrt{3}}{2} \end{vmatrix} \begin{vmatrix} i_a \\ i_b \\ i_c \end{vmatrix} \tag{23}$$

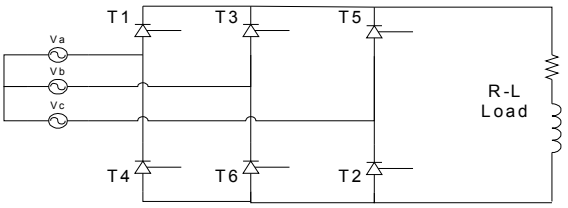

Fig. A. Schematic diagram for three-phase controlled converter

Then p and q are calculated from α-β domain voltages and current as shown in (24):

$$\begin{vmatrix} p \\ q \end{vmatrix} = \begin{vmatrix} v_\alpha & v_\beta \\ -v_\beta & v_\alpha \end{vmatrix} \begin{vmatrix} i_\alpha \\ i_\beta \end{vmatrix} \tag{24}$$

The instantaneous p and q can be decomposed into the following:

$$p = \bar{p} + \tilde{p} \tag{25}$$

$$q = \bar{q} + \tilde{q} \tag{26}$$

where $\bar{p}$ is the constant part of p (which is coming from the fundamental components), $\tilde{p}$ is the oscillating part of p (which is coming from harmonics), and in similar fashion $\bar{q}$ and $\tilde{q}$ for the q.

In this paper, the used compensation strategy is called sinusoidal current strategy. Here both oscillating parts $\tilde{p}$ and $\tilde{q}$ are extracted by using the moving average technique. The resulting reference power signal contains $\tilde{p}$ plus p_{loss} (additional power losses present) and $\tilde{q}$ is shown as p_{ref} and q_{ref} in (30) and (31), respectively:

$$p_{ref} = \tilde{p} + p_{loss} \tag{27}$$

$$q_{ref} = \tilde{q} \tag{28}$$

The reference current in α-β domain can be calculated by:

$$\begin{vmatrix} i_{\alpha ref} \\ i_{\beta ref} \end{vmatrix} = \begin{vmatrix} v_\alpha & v_\beta \\ -v_\beta & v_\alpha \end{vmatrix}^{-1} \begin{vmatrix} p_{ref} \\ q_{ref} \end{vmatrix} \tag{29}$$

Then the reference current in a-b-c domain can be calculated as:

$$\begin{vmatrix} i_{aref} \\ i_{bref} \\ i_{cref} \end{vmatrix} = \sqrt{\frac{2}{3}} \begin{vmatrix} 1 & 0 \\ -\frac{1}{2} & \sqrt{\frac{3}{2}} \\ -\frac{1}{2} & -\sqrt{\frac{3}{2}} \end{vmatrix} \begin{vmatrix} i_{\alpha ref} \\ i_{\beta ref} \end{vmatrix} \tag{30}$$

REFERENCES

[1] M. Izhar, C. M. Hadzer, S. Masri and S. Idris, "A study of the fundamental principles to power system harmonic," *Proc. of Power Engineering Conference*, pp. 225-232, 2003.

[2] J. S. Subjak Jr. and J. S. McQuilkin, "Harmonics-causes, effects, measurements, and analysis: an update," *IEEE Transactions on Industry Applications,* vol. 26, no. 6, pp. 1034-1042, 1990.

[3] Sumaryadi, H. Gumilang and A. Suslilo, "Effect of power system harmonic on degradation process of transformer insulation system," *IEEE Conference on Properties and Applications of Dielectric Materials,* pp. 261-264, 2009.

[4] S. Rahmani, A. Hamadi and K. Al-Haddad, "A new combination of shunt hybrid power filter and thyristor controlled reactor for harmonics and reactive power compensation," *IEEE Conference on Electrical Power & Energy Conference*, pp. 1-6, 2009.

[5] H. Akagi, "New trends in active filters for improving power quality," *Power Electronics, Drives and Energy Systems for Industrial Growth Conference*, pp. 417-425, 1996.

[6] B. Singh, K. Al-Haddad and A. Chandra, "A review of active filters for power quality improvement," *IEEE Transactions on Industrial Electronics,* vol. 46, no. 5, pp. 960-971, 1999.

[7] V. Khadkikar, "Enhancing electric power quality using UPQC: a comprehensive overview," *IEEE Transactions on Power Electronics,* vol. 27, no. 5, pp. 2284-2297, 2011.

[8] D. Chen and S. Xie, "Review of the control strategies applied to active power filters," *IEEE Conference on Electric Utility Deregulation, Restructuring and Power Technologies,* pp. 666-670, 2004.

[9] W. Lenwari and M. Odavic, "A comparative study of two high performance current control techniques for three-phase shunt active power filters," *Power Electronics and Drive Systems Conference,* pp. 962-966, 2009.

[10] S. Rahmani, K. Al-Haddad, H. Y. Kanaan and F. Fnaiech, "A comparative study of two PWM techniques for single-phase shunt active power filters employing direct current control strategy," *Power Electronics Specialists Conference,* pp. 2758-2763, 2005.

[11] R. A. Kantaria, S. K. Joshi and K. R. Siddhapura, "A novel hysteresis control technique of VSI based STATCOM," *Power Electronics India Conference,* pp. 1-5, 2011.

[12] Y. Dongmei, G. Qingding, H. Qing and L. Chunfang, "A novel DSP based current controller with fuzzy variable-band hysteresis for active power filters," *Transmission and Distribution Conference and Exhibition: Asia and Pacific,* pp. 1-5, 2005.

[13] S. R. Prusty, S. K. Ram, B. D. Subudhi and K. K. Mahapatra, "Performance analysis of adaptive band hysteresis current controller for shunt active power filter," *Emerging Trends in Electrical and Computer Technology Conference,* pp. 425-429, 2011.

[14] D. G. Holmes, R. Davoodnezhad and B. P. McGrath, "An improved three phase variable band hysteresis current regulator," *IEEE Conference on Power Electronics*, pp. 2274-2281, 2011.

[15] Y. Ounejjar, K. Al-haddad and L. Dessaint, "A novel six-band hysteresis control for the packed U cells seven-level converter: experimental validation," *IEEE Transactions on Industrial Electronics,* vol. 59, no. 10, pp. 3808-3816, 2011.

[16] A. Naik, B. C. Babu and A. K. Panda, "Improved performance of adaptive hysteresis current controller based vector control of PMSM drive system," *IEEE Students' Technology Symposium*, pp. 303-309, 2011.

[17] B. K. Bose, "An adaptive hysteresis-band current control technique of a voltage-fed pwm inverter for machine drive system," *Industrial Electronics Society Annual Conference,* pp. 684-690, 1988.

[18] L. Malesani, P. Mattavelli and P. Tomasin, "High-performance hysteresis modulation technique for active filters," *IEEE Transactions on Power Electronics,* vol. 12, no. 5, pp. 876-884, 1997.

[19] Kazmierkowski, Marian P., and L. Malesani. "Current control techniques for three-phase voltage-source PWM converters: a survey," *IEEE Transactions on Industrial Electronics,* vol. 45, no. 5, pp. 691-703, 1998.

[20] L. Malesani, P. Mattavelli and P. Tomasin, "Improved constant-frequency hysteresis current control of VSI inverters with simple feedforward bandwidth prediction," *IEEE Transactions on Industry Applications,* vol. 33, no. 5, pp. 1194-1202, 1997.

[21] L. P. Ling and N. A. Azli, "SVM based hysteresis current controller for a three phase active power filter," *Power and Energy Conference,* pp. 132-136, 2004.

[22] J. A. Suul, K. Ljokelsoy, T. Midtsund and T. Undeland, "Synchronous reference frame hysteresis current control for grid converter applications," *Power Electronics and Motion Control Conference*, pp. 111-119, 2010.

[23] G. Tsengenes and G. Adamidis, "An improved current control technique for the investigation of a power system with a shunt active filter," *Power Electronics, Electrical Drives, Automation and Motion Symposium*, pp. 239-244, 2010.

[24] L. Jun and W. Dazhi, "Study and simulation of a novel hysteresis current control strategy," *Intelligent Computation Technology and Automation Conference,* pp. 306-309, 2009.

[25] L. Xia, D. Taihang and T. Shengxue, "A fuzzy logic variable hysteresis band current control technique for three phase shunt active power filter," *Control, Automation and Systems Engineering Conference,* pp. 1-4, 2011.

[26] W. Dazhi, J. Guoqing, L. Jun, S. Hualong, L. Shengli and S. Keling, "A novel hysteresis current control strategy based on neural network," *Computer Design and Applications Conference,* pp. 369-372, 2010.

[27] D. Wenjin, L. Qingsheng and C. Xiangjie, "Research on harmonics suppression and reactive power compensation for power system," *Intelligent Information Technology Application Symposium,* pp. 110-112, 2009.

[28] L. Qiong, X. Qiang and R. Wu. "An improved predictive current method for permanent magnet synchronous motors," *IEEE Transportation Electrification Asia-Pacific Conference and Expo,* pp. 1-6, 2014.

[29] Q. Mohammed, P. Kanjiya and V. Khadkikar, "Artificial-neural-network-based phase-locking scheme for active power filters," *IEEE Transactions on Industrial Electronics,* vol. 61, no. 8, pp. 3857-3866, 2014.

[30] A. Emadi, A. Nasiri and S. B. Bekiarov, *Uninterruptible Power Supplies and Active Filters*. Boca Raton: CRC Press, 2005.

[31] H. Akagi, *Instantaneous Power Theory and Applications to Power Conditioning.* Hoboken: John Wiley Sons, 2007.